MODELLING AND OPTIMIZATION OF A DEFORMABLE MIRROR FOR LASER BEAM CONTROL

Philip W. Loveday[1,*], Craig S. Long[2,*], Andrew Forbes[†] and Kevin Land[‡]

[*] Sensor Science & Technology, CSIR Material Science and Manufacturing, Box 395, Pretoria 0001, South Africa, [1]ploveday@csir.co.za, [2]clong@csir.co.za
[†] Mathematical Optics, CSIR National Laser Centre, Box 395, Pretoria 0001, South Africa, aforbes1@csir.co.za
[†] School of Physics, University of KwaZulu-Natal, Private Bag X54001, Durban 4000, South Africa
[‡] Manufacturing Science & Technology, CSIR Material Science and Manufacturing, Box 395, Pretoria 0001, South Africa, kland@csir.co.za

Key words: Deformable mirror, laser beam control, piezoelectric unimorph

Abstract

An intra-cavity adaptive mirror is required to compensate for time-dependent phase aberrations to the laser beam, such as those caused by thermal lensing. A piezoelectric unimorph design can provide a small, low-cost deformable mirror for this application. The unimorph consists of a metallic disc, with a mirror finish, bonded to a piezoelectric disc. In adaptive optics the deformations that the mirror is required to perform are described by the Zernike polynomials, which are a complete set of orthogonal functions. The challenge is to design a device that can represent selected polynomials as accurately as possible with specified amplitude. Numerical modelling is required to predict the deformation shapes that can be achieved by a unimorph mirror with a particular electrode pattern. The results from a Rayleigh-Ritz model and a finite element model employing elements including rotational degrees of freedom were compared to results from a conventional finite element model. The Rayleigh-Ritz model, which used the Zernike polynomials directly to describe the displacements, produced a small model (stiffness matrix dimension equal to the number of polynomials used) that predicts the deformations of the piezoelectric mirror with remarkable accuracy. While this method requires some effort to implement and is not very flexible, it does provide insight into the operation of the deformable mirror and can be used to optimize the design in an elegant manner. The finite element model including rotational degrees of freedom is more efficient than the conventional finite element model but retains the flexibility of this model. This method was applied to model a prototype deformable mirror and produced good agreement with experimental results.

1. INTRODUCTION

Adaptive optics is routinely used in large earth based telescopes to correct for the effects of atmospheric turbulence. These systems use large arrays of mirrors individually controlled by sets of piezoelectric stack actuators and are therefore very expensive. For intra-cavity laser beam control, a smaller, lower-cost deformable mirror is required. This mirror can be used to correct for time-dependent phase aberrations to the laser beam, such as those caused by thermal lensing in solid state lasers. A piezoelectric unimorph design, such as that depicted in figure 1, is suitable for this application [1].

The unimorph consists of a metallic disc, with a mirror finish, bonded to a piezoelectric disc. When a voltage is applied to the piezoelectric disc the induced strains in the plane of the disc cause bending of the unimorph. In this way relatively large displacements, compared to the 10.6 μm wavelength of a CO_2 laser, can be obtained from a small and relatively inexpensive device. The electrode on the free surface of the piezoelectric disc can be divided into numerous segments, which can each have a different voltage applied. In this way the mirror can be deformed into a more complex shape.
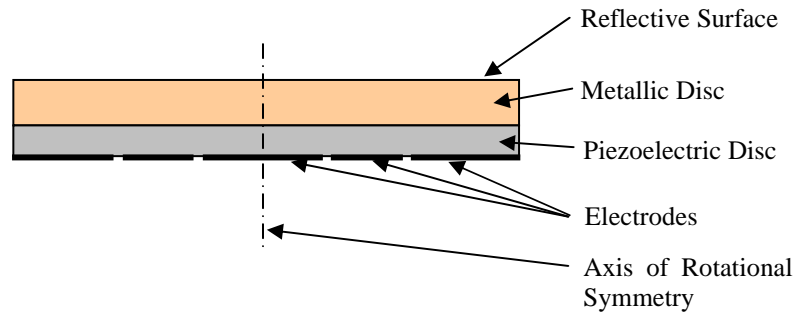
Figure 1. Unimorph deformable mirror configuration.

In adaptive optics the imperfections in the optical system and therefore the deformations that the mirror is required to perform are described by Zernike polynomials. The Zernike polynomials form a complete set of orthogonal functions on the unit circle. The challenge is to design a device that can represent selected polynomials as accurately as possible with specified amplitude. Numerical modelling is required to predict the deformation shapes that can be achieved by a particular electrode pattern.

In this paper three numerical models are developed and the results are compared. Firstly, a Rayleigh-Ritz model, using the Zernike polynomials directly to describe the motion of the mirror is developed in section 2. The Rayleigh-Ritz model has the advantage that the deformations are directly expressed in terms of the Zernike polynomials so no curve fitting is required. A finite element modelling approach, based on specially formulated hybrid axisymmetric piezoelectric elements with rotational degrees of freedom, is presented in section 3. A least-squares fit of the deformation of the mirror surface is carried out in order to determine which of the Zernike polynomials are being excited. A second finite element model, this time using the commercial code COMSOL, was prepared for comparison. A first prototype device was constructed and surface displacements were measured using a laser vibrometer, as detailed in section 4. The results of the three models are compared in section 5.1 while the first finite element model is compared to experimental measurements in section 5.2. Optimization of the electrode pattern to excite a particular polynomial is briefly described in section 6.

2. RAYLEIGH – RITZ MODEL FORMULATION

The Rayleigh-Ritz method was applied to a cantilever beam with attached piezoelectric ceramic patches by Hagood et al. in 1990 [2] and has become popular for piezoelectric structures since then. The method is based on Hamilton's principle for coupled electromechanical systems and is described in detail in [2] so only the additional details required to apply the method to the unimorph are described here. The method was applied to the geometry shown in figure 2.
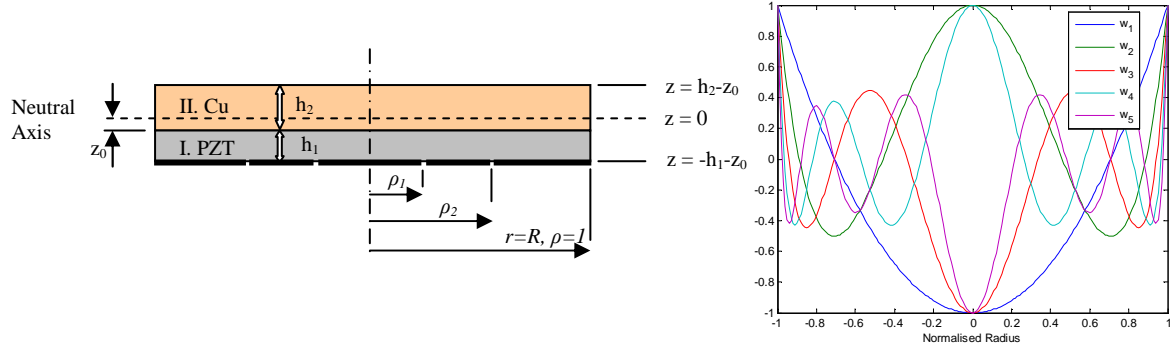
Figure 2. Unimorph mirror dimensions and Zernike polynomials used in modelling.

To apply the method one is required to select a set of assumed displacement distributions and electrical potential distributions. In this case we use the Zernike polynomials, shown in figure 2, as the assumed displacement distributions. The displacement may be written as a superposition of assumed displacement functions with unknown coefficients,

$$w(r,t) = W(r)a(t) = R\{w_1(\rho) \quad \cdots \quad w_n(\rho)\}\begin{Bmatrix} a_1(t) \\ \vdots \\ a_n(t) \end{Bmatrix},$$

(1)

where, R is the radius of the disc, $w_1(\rho)$ is the first Zernike polynomial, ρ is the non-dimensionalised radius and $a_1(t)$ is the amplitude coefficient for the first polynomial, which has to be determined. The first five axisymmetric deformation polynomials as listed below were used in the modelling.

$$w_1 = -1 + 2\rho^2$$
$$w_2 = 1 - 6\rho^2 + 6\rho^4$$
$$w_3 = -1 + 12\rho^2 - 30\rho^4 + 20\rho^6$$
$$w_4 = 1 - 20\rho^2 + 90\rho^4 - 140\rho^6 + 70\rho^8$$
$$w_5 = -1 + 30\rho^2 - 210\rho^4 + 560\rho^6 - 630\rho^8 + 252\rho^{10}$$

(2)

Next, we require a strain-displacement operator for the particular structure being modelled. If we limit ourselves to the case of axisymmetric bending displacements of a circular plate the appropriate strain-displacement operator is given in equation 3, where L_w is the strain-displacement operator, w is the displacement normal to the neutral axis and z is the distance from the neutral axis.

$$\begin{Bmatrix} \varepsilon_r \\ \varepsilon_\theta \end{Bmatrix} = L_w w = \begin{Bmatrix} -z\dfrac{\partial^2}{\partial r^2} \\ -\dfrac{z}{r}\dfrac{\partial}{\partial r} \end{Bmatrix} w$$

(3)

The strain basis functions are then written in terms of the unknown coefficients as

$$S(r,t) = N_w(r)a(t) = L_w W(r)a(t) .$$

(4)

The stiffness matrix is obtained by integration over the volume of the structure,

$$K = \int_v N_w{}^T c N_w dv$$

(5)

In a similar fashion the electrical potential field is described by assumed functions. As this is a thin piezoelectric disc it will be assumed that the electric field varies linearly through the thickness of the disc. We set the voltage on the electrode contacting the copper to be zero and

the voltages on the ith free electrode segment to be v_i. We assume that there is no radial variation of the electrical potential under an electrode segment. The electrical potential under electrode segment i is therefore, $v_i(z,t) = -v_i(t)(z+z_0)/h_1$.

The electric field is simply the negative of the gradient of this ie., $\psi_i(t) = v_i(t)/h_1$ and the field is written as,

$$\psi(t) = [1/h_1 \quad \cdots \quad 1/h_1] \begin{bmatrix} v_1(t) \\ \vdots \\ v_m(t) \end{bmatrix} = N_v v(t) \tag{6}$$

The piezoelectric coupling matrix is then,

$$\Theta = \int_v N_w{}^T e N_v dv . \tag{7}$$

The mass matrix and capacitance matrix can be implemented if we wish to compute natural frequencies.

$$C_p = \int_v N_v{}^T \varepsilon N_v dv \tag{8}$$

$$M = \int_v \rho W^T W dv \tag{9}$$

The coupled electromechanical equations are then,

$$Ka - \Theta v = f$$
$$\theta^T a + C_p v = q \tag{10}$$

Special attention must be paid to the piezoelectric material properties used in the model. The properties listed by piezoelectric ceramic manufacturers are for three dimensional piezoelectric problems. In the thin piezoelectric disc used in the unimorph we assume that the stress in the thickness direction of the disc is zero but this strain is non zero. The in-plane stresses are non-zero. The strains and stresses can be related by retaining the relevant terms in $S = s^E T + d^t E$ as follows.

$$\begin{Bmatrix} S_1 \\ S_2 \end{Bmatrix} = \begin{bmatrix} s_{11}{}^E & s_{12}{}^E \\ s_{12}{}^E & s_{22}{}^E \end{bmatrix} \begin{Bmatrix} T_1 \\ T_2 \end{Bmatrix} + \begin{Bmatrix} d_{31} \\ d_{31} \end{Bmatrix} E_3 \tag{11}$$

This relation can be manipulated to the form required for the above development, ie.,

$$T = c^E S - e^t E ,$$

with $c^E = \dfrac{1}{s_{12}^{E\,2} - s_{11}^{E\,2}} \begin{bmatrix} -s_{11}{}^E & s_{12}{}^E \\ s_{12}{}^E & -s_{11}{}^E \end{bmatrix}$ and $e^t = \dfrac{1}{s_{12}^E + s_{11}^E} \begin{Bmatrix} d_{31} \\ d_{31} \end{Bmatrix}$.

The position of the neutral axis (z_0) can be calculated by minimizing the strain energy or the flexural rigidity and the result is,

$$z_0 = \frac{h_2{}^2 E_2 (1 - v_1{}^2) - h_1{}^2 E_1 (1 - v_2{}^2)}{2[h_2 E_2 (1 - v_1{}^2) + h_1 E_1 (1 - v_2{}^2)]} , \tag{12}$$

where for the piezoelectric material, $v_1 = \dfrac{c_{12}}{c_{11}}$ and $E_1 = c_{11}(1 - v^2)$.

The position of the neutral axis is required during the integration to form the stiffness matrix. The integrations, required to form the matrices, can be performed analytically to obtain expressions for each term in the matrices. The matrix elements therefore contain the design dimensions (R, h_1, h_2, ρ_1, ρ_2) and material properties explicitly. These integrations were

conveniently performed in the freeware package 'Maxima' and the resulting expressions were copied into Matlab.

3. ELEMENTS WITH ROTATIONAL DOF'S AND POLYNOMIAL EXTRACTION

To compare the numerical procedure based on the Rayleigh-Ritz method proposed in the previous section, a more conventional finite element analysis is conducted. For the purposes of this comparison, an axisymmetric finite element model using specially developed finite elements with rotational degrees of freedom is employed. These elements have been shown to be especially well suited to bending-dominated problems [3].

The variational formulation employs the skew-symmetric part of the stress tensor as a Lagrange multiplier to enforce the continuum mechanics definition of rotations in terms of displacement gradient, see (13). The stress tensor is therefore not *a priori* assumed to be symmetric. The specific elastic elements used in this analysis are based on the functional

$$\Pi_{\gamma}(\mathbf{u}, \boldsymbol{\psi}, \text{skew}\,\boldsymbol{\sigma}) = \frac{1}{2}\int_{\Omega} \mathbf{c}\,\text{symm}\,\nabla\mathbf{u}\cdot\text{symm}\,\nabla\mathbf{u}\,\mathrm{d}V + \int_{\Omega}(\text{skew}\,\nabla\mathbf{u} - \boldsymbol{\psi})\cdot\text{skew}\,\boldsymbol{\sigma}\,\mathrm{d}V -$$
$$\frac{1}{2\gamma}\int_{\Omega}|\text{skew}\,\boldsymbol{\sigma}|^2\,\mathrm{d}V - \int_{\Omega}\mathbf{f}\cdot\mathbf{u}\,\mathrm{d}V + \text{Boundary terms.} \tag{13}$$

More detail regarding the elastostatic elements may be found in [3]. In order to model the piezoelectrically driven deformable mirror, the elastostatic elements were extended to account for the piezoelectric effect. For brevity, the functional on which the piezoelectric elements with rotational degrees of freedom are based is not given here.

As mentioned previously, in adaptive optics the spatial deformations that the mirror is required to perform are described using Zernike polynomials, which form a complete set of orthogonal functions over the unit circle. The form of the polynomials used in this section is given by:

$$Z_n^m(\rho, \varphi) = R_n^m \cos(m\varphi), \tag{14}$$

with $0 \le \rho \le 1$, $0 \le \varphi \le 2\pi$, and where

$$R_n^m = \sum_{k=0}^{(n-m)/2}(-1)^k \rho^{n-2k}\frac{(n-k)!}{k!\left(\left(n+\frac{m}{2}-k\right)!\left(n-\frac{m}{2}-k\right)!\right)!}. \tag{15}$$

Note that R_n^m is only defined for (n-m) positive and even. Furthermore, due to the symmetry of the problem, only axisymmetric polynomials are considered (i.e. m=0). For brevity, we will denote this subset of Zernike polynomials as follows

$$Z_i \equiv Z_{n=2i}^{m=0}, \quad i=0,1,2,\dots. \tag{16}$$

Note that in (2) $w_i \equiv Z_i$.

A finite element analysis of the structure described in Figure 2 was performed, and from this analysis, the vertical displacements of the surface were extracted. Figure 3 depicts an example result using the finite element method described above. Now a procedure is required to determine which of the Zernike polynomials are excited.
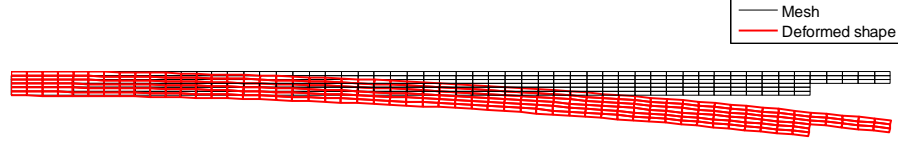
Figure 3. Typical result using the finite element method, depicting the discretisation and deformed shape.

To this end, a least-squares fit of the surface displacements is employed, i.e. we minimize the function

$$\chi^2 = \sum_{i=1}^{N} \left[y_i - \sum_{k=0}^{M} a_k Z_k(r_i) \right]^2 , \qquad (17)$$

where y_i is the ith of the N surface nodal displacements. The minimization is carried out using the procedure described in [1]. The output of this process is a vector of the coefficients a_k which scale the magnitude of the M non-constant Zernike polynomials.

Figure 4 illustrates a typical result of the polynomial fitting procedure using various numbers of (non-constant) Zernike polynomials, i.e. $M = 3, 5, 10$ and 20. The figure demonstrates that the error in the fit decreases as the number of polynomials increases, indicating that the procedure is reliable.
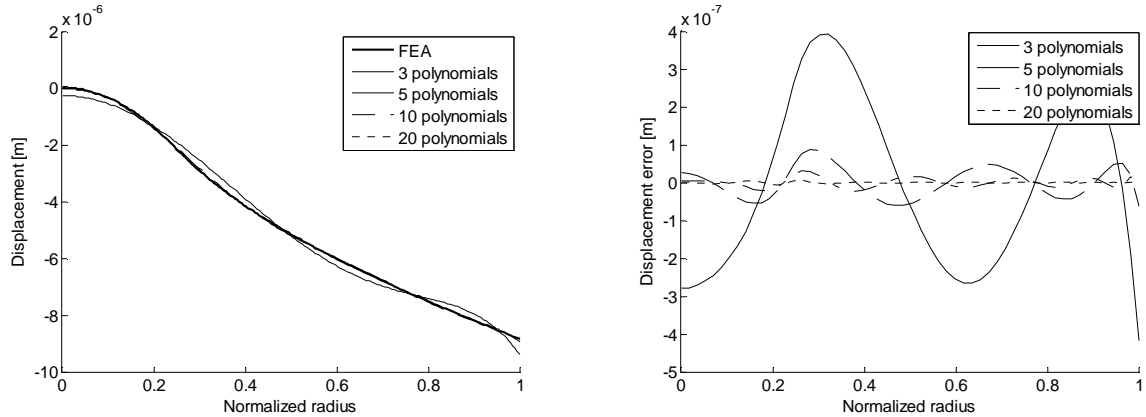
(a) Zernike polynomial fit of finite element results. (b) Error of Zernike polynomial fit.
Figure 4. Example of Zernike polynomial fitting of finite element prediction of mirror surface using voltage $V_{\text{drive}}=[200{:}0{:}0]$.

4. EXPERIMENTAL DETAILS

In order to assess the practicality of the proposed numerical models, a physical prototype was constructed. The prototype unimorph-type deformable mirror consists of a 40 mm diameter, 0.3 mm thick, PZT4 piezoelectric ceramic disc bonded to a copper disc 44 mm in diameter and 0.3 mm thick. The slightly larger diameter of the copper provides a surface onto which is attached a grounding wire as shown in Figure 5. The free electrode on the piezoelectric disc is segmented into three concentric rings. The electrode patterning was carried out using laser ablation with an excimer laser. The unimorph was driven by applying a harmonic voltage excitation to the segmented electrodes. Point deformations of the disc were measured using a Polytec laser vibrometer.

(a) Deformable mirror prototype (front view).

(b) Deformable mirror prototype (rear view).

Figure 5. Prototype deformable mirror.

5. COMPARISON OF RESULTS

In this section results of the Rayleigh-Ritz and finite element numerical models are compared. For completeness, a commercial finite element code, Comsol Multiphysics, is also used in the comparison. Results from the first finite element model are then compared to experimental results derived from the prototype device described in Section 4.

5.1 Comparison of Rayleigh-Ritz, R-DOF FE and Commercial FE models

Firstly, the numerical models are compared without considering an experimental comparison. In this case, both the piezoceramic and the copper discs have the same diameter. A model with three annular electrodes was used for the comparison. A 40 mm diameter device made from a 0.5 mm thick PZT4 disc (s_{11}^E=12.3e-12 m^2/N; s_{12}^E =-4.05e-12 m^2/N; d_{31}= -123e-12 m/V, ε_{33}^E = 635x8.85e-12 F/m) bonded to a 0.5 mm thick copper disc (E=110 GPa, ν=0.33) was modelled. The extent of the first electrode is from $\rho=0$ to ρ_1, the second from $\rho= \rho_1$ to ρ_2, and the third from $\rho= \rho_2$ to 1. The electrodes were positioned where they would be expected to best excite the third Zernike polynomial, i.e. ρ_1 =0.27 and ρ_2 =0.72. These points are found by solving $\dfrac{\partial^2 w_3}{\partial \rho^2} = 0$. This estimate neglects the influence of circumferential strains and a

better estimate of the optimal electrode positions is presented in section 6.

The cases of 200V applied to each electrode individually were computed. The voltage on the individual segments is contained in the vector $V_{drive} = [V_1 : V_2 : V_3]$, where V_i is the voltage on the ith electrode segment. The displacements are illustrated in figure 6 and the coefficients of the Zernike polynomials are listed in table 1.

(a) $V_{drive}=[200:0:0]$.   (b) $V_{drive}=[0:200:0]$.   (c) $V_{drive}=[0:0:200]$.
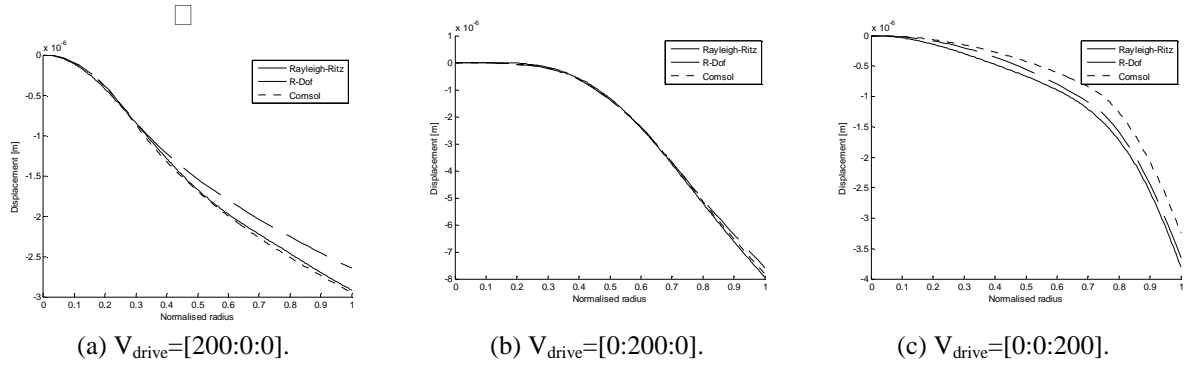
Figure 6. Comparison of mirror surface displacement prediction using different numerical models.

Voltage (V_{drive})	Polynomial number	Rayleigh-Ritz	R-DOF element model	Comsol Multiphysics
[200 : 0 : 0]	a_1 [μm]	-1.170	-1.042	-1.187
	a_2 [μm]	0.472	0.429	0.491
	a_3 [μm]	-0.258	-0.234	-0.257
[0 : 200 : 0]	a_1 [μm]	-4.436	-4.204	-4.343
	a_2 [μm]	-0.002	0.055	0.001
	a_3 [μm]	0.441	0.404	0.427
[0 : 0 : 200]	a_1 [μm]	-1.729	-1.696	-1.485
	a_2 [μm]	-0.471	-0.484	-0.519
	a_3 [μm]	-0.183	-0.170	-0.175

Table 1. Comparison of the predicted Zernike polynomial coefficients using different numerical models.

5.2 Comparison of finite element models and experimental data

The first FE model is now compared to experimental data. Due to the practical issue of attaching the grounding wire to the copper disc, the copper disc was slightly larger than the PZT4 disc. The Rayleigh-Ritz model was not extended to include this detail. Due to the flexibility of the finite element method when compared to the Rayleigh-Ritz method, and the close agreement between the numerical models, only a finite element analysis is carried out for this geometry. The results for driving each electrode are shown in figure 7 and the coefficient of the Zernike polynomials are listed in table 2. It is noted that the shape of the deformations are very similar but the model over predicts the deformation. It is believed that this is because the material properties of the piezoelectric disc used in the experiment are not known accurately and differ from those used in the model. The coefficients of the polynomials which are strongly excited are predicted with reasonable accuracy. Those that have small response show large percentage errors although the absolute error is acceptable.

(a) $V_{drive}=[100:0:0]$. (b) $V_{drive}=[0:100:0]$. (c) $V_{drive}=[0:0:100]$.
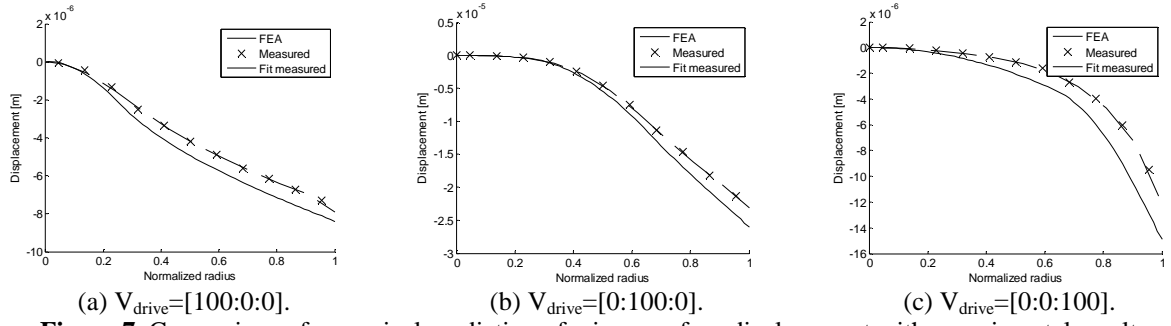
Figure 7. Comparison of numerical prediction of mirror surface displacement with experimental results.

Voltage (V_{drive})	Polynomial coefficient	Experimental [μm]	FEA [μm]	Percentage difference [%]
	a_1	-3.08	-3.22	-4.35
[100 0 0]	a_2	1.10	1.32	-16.67
	a_3	-0.68	-0.75	-9.33
	a_1	-12.67	-14.31	-11.46
[0 100 0]	a_2	0.73	0.97	-24.72
	a_3	1.10	1.17	-5.98
	a_1	-5.45	-7.30	-25.34
[0 0 100]	a_2	-2.04	-2.15	-5.12
	a_3	-0.55	-0.28	96.43

Table 2. Comparison of the predicted Zernike polynomial coefficients using FEA and experimental results.

6. DEFORMABLE MIRROR OPTIMIZATION

The thickness of the device has a strong influence on the deformations that can be obtained with thin devices producing greater deformations. Practical difficulties in making a thin device which is still flat limit the thickness of the device. One area where the designer has freedom is in selecting the electrode configuration. In this section it is briefly shown how the Rayleigh-Ritz model can be used to optimize the electrode configuration.

Consider the problem of optimizing the layout of the three electrodes to maximize the deformation of the third Zernike polynomial. The displacement of the mirror to a voltage vector v in terms of the Zernike polynomials may be written directly from (10) as $a = K^{-1}\Theta v$. We have two design variables ρ_1 and ρ_2 and we want to maximize the coefficient of the third polynomial a_3. We note that the stiffness matrix and voltage vector are not functions of these variables therefore, $\dfrac{\partial a}{\partial \rho_i} = K^{-1}\dfrac{\partial \Theta}{\partial \rho_i}v$. We know that to excite the third polynomial the voltage applied to the middle electrode will have opposite polarity to that applied to the inner and outer electrodes therefore we can set $v = V_{max}\begin{bmatrix} 1 & -1 & 1 \end{bmatrix}^T$. In addition, we are only interested in the coefficient of the third polynomial, which can be extracted as follows:

$$\frac{\partial a_3}{\partial \rho_i} = \begin{bmatrix} 0 & 0 & 1 & 0 & 0 \end{bmatrix} K^{-1}\frac{\partial \Theta}{\partial \rho_i}\begin{bmatrix} 1 & -1 & 1 \end{bmatrix}^T .$$

If we perform this computation and set the result to zero we obtain the following equation,

$793800\rho^9 - 2114560\rho^7 + 1901880\rho^5 - 633744\rho^3 + 52804\rho = 0$. It is interesting to note that the above equation is produced for differentiation with respect to either ρ_1 or ρ_2 and there is no coupling between these variables in the piezoelectric coupling matrix. The two solutions in the range $0 < \rho < 1$ are $\rho_1 = 0.35$ and $\rho_2 = 0.7377$. These values of ρ_1 and ρ_2 were checked by computing the performance of configurations around this point and it was found that these are indeed the optimal positions for the two electrode divisions. The predicted deformation in the third polynomial, using this optimal electrode configuration, is approximately 10% greater than that predicted with the previous electrode configuration ($\rho_1 = 0.27$ and $\rho_2 = 0.72$).

7. CONCLUSIONS

The three numerical models compared in this paper produced very similar results. The Rayleigh-Ritz method produces a small model (stiffness matrix dimension equal to the number of polynomials used) that predicts the deformations of the piezoelectric mirror with remarkable accuracy. This method also provides insight into the operation of the device and can be used to optimize the design in an elegant manner. The method is not very flexible if different geometries and boundary conditions are required and does require considerable time to implement although the use of symbolic mathematical software can reduce the time required. The results from this model would provide a good starting point for FE modelling. The FE method including rotational degrees of freedom is more efficient than the conventional FE method available in commercial software but retains the flexibility of the method for axisymmetric problems. Good agreement was obtained between experimental measurements and the FE method including rotational degrees of freedom.

References

1. Ellis E.M., *Low-cost bimorph mirrors in adaptive optics*, Ph.D. thesis, Imperial College of Science, Technology and Medicine, University of London, 1999.
2. Hagood, N.W., Chung, W. and von Flotow, A., Modeling of piezoelectric actuator dynamics for active structural control, *Journal of Intelligent Material Systems and Structures*, 1(3), 327-354, 1990.
3. Long, C.S., Loveday, P.W. and Groenwold, A.A., Axisymmetric solid-of-revolution finite elements with rotational degrees of freedom, *Finite Elements in Analysis and Design*, Submitted 2007.